PLOS ONE

RESEARCH ARTICLE

Multi-Site Clinical Evaluation of DW-MRI as a Treatment Response Metric for Breast Cancer Patients Undergoing Neoadjuvant Chemotherapy

Craig J. Galbán[1], Bing Ma[1], Dariya Malyarenko[1], Martin D. Pickles[5], Kevin Heist[1], Norah L. Henry[2], Anne F. Schott[2], Colleen H. Neal[1], Nola M. Hylton[6], Alnawaz Rehemtulla[3], Timothy D. Johnson[4], Charles R. Meyer[1], Thomas L. Chenevert[1], Lindsay W. Turnbull[5], Brian D. Ross[1]*

1 Departments of Radiology, University of Michigan, Ann Arbor, Michigan, United States of America, **2** Departments of Internal Medicine, University of Michigan, Ann Arbor, Michigan, United States of America, **3** Departments of Radiation Oncology, University of Michigan, Ann Arbor, Michigan, United States of America, **4** Departments of Biostatistics, University of Michigan, Ann Arbor, Michigan, United States of America, **5** Centre for MR Investigations, Hull York Medical School, University of Hull, Hull, United Kingdom, **6** Department of Radiology, University of California San Francisco, San Francisco, California, United States of America

* bdross@umich.edu

OPEN ACCESS

Citation: Galbán CJ, Ma B, Malyarenko D, Pickles MD, Heist K, Henry NL, et al. (2015) Multi-Site Clinical Evaluation of DW-MRI as a Treatment Response Metric for Breast Cancer Patients Undergoing Neoadjuvant Chemotherapy. PLoS ONE 10(3): e0122151. doi:10.1371/journal.pone.0122151

Academic Editor: Adam J Schwarz, Indiana University, UNITED STATES

Received: July 1, 2014

Accepted: February 18, 2015

Published: March 27, 2015

Data Availability Statement: All relevant data are within the paper.

Funding: Funds were provided by NIH grants U01CA151235, U01CA166104 and P01CA087634 as well as Yorkshire Cancer Research to establish and fund the Hull MRI Centre and Cancer Research UK who funded the NeoComice study. The funders had no role in study design, data collection and analysis, decision to publish, or preparation of the manuscript.

Competing Interests: The authors of this manuscript have the following competing interests. BDR, TLC,

Abstract

Purpose

To evaluate diffusion weighted MRI (DW-MR) as a response metric for assessment of neoadjuvant chemotherapy (NAC) in patients with primary breast cancer using prospective multi-center trials which provided MR scans along with clinical outcome information.

Materials and Methods

A total of 39 patients with locally advanced breast cancer accrued from three different prospective clinical trials underwent DW-MR examination prior to and at 3–7 days (Hull University), 8–11 days (University of Michigan) and 35 days (NeoCOMICE) post-treatment initiation. Thirteen patients, 12 of which participated in treatment response study, from UM underwent short interval (<1hr) MRI examinations, referred to as "test-retest" for examination of repeatability. To further evaluate stability in ADC measurements, a thermally controlled diffusion phantom was used to assess repeatability of diffusion measurements. MRI sequences included contrast-enhanced T1-weighted, when appropriate, and DW images acquired at b-values of 0 and 800 s/mm^2. Histogram analysis and a voxel-based analytical technique, the Parametric Response Map (PRM), were used to derive diffusion response metrics for assessment of treatment response prediction.

AFS, AR and CJG have the following patents (Systems and methods for tissue imaging US8768431B2 and Imaging systems, computer, program product and method for detecting changes in rates of water diffusion in a tissue using magnetic resonance imaging (MIR) US6567684B1) and disclosures to the University of Michigan related to the underlying technologies described in this report which have been licensed to Imbio, LLC, a company in which BDR and AR have a financial interest. This does not alter the authors' adherence to all PLOS ONE policies on sharing data and materials as detailed in the guide for authors.

Results

Mean tumor apparent diffusion coefficient (ADC) values generated from patient test-retest examinations were found to be very reproducible ($|\Delta ADC| < 0.1x10^{-3}mm^2/s$). This data was used to calculate the 95% CI from the linear fit of tumor voxel ADC pairs of co-registered examinations ($\pm 0.45x10^{-3}mm^2/s$) for PRM analysis of treatment response. Receiver operating characteristic analysis identified the PRM metric to be predictive of outcome at the 8–11 (AUC = 0.964, p = 0.01) and 35 day (AUC = 0.770, p = 0.05) time points ($p < .05$) while whole-tumor ADC changes where significant at the later 35 day time interval (AUC = 0.825, p = 0.02).

Conclusion

This study demonstrates the feasibility of performing a prospective analysis of DW-MRI as a predictive biomarker of NAC in breast cancer patients. In addition, we provide experimental evidence supporting the use of sensitive analytical tools, such as PRM, for evaluating ADC measurements.

Introduction

An important component in the treatment of primary breast cancer is the use of adjuvant systemic therapy. This allows for the opportunity to provide for a reduction in the risk of recurrence and death [1–5]. In breast cancer patients, randomized studies have found that preoperative chemotherapy provides a similar survival benefit from a particular treatment regimen which is similar to post-operative therapy [5]. Preoperative therapy is an important approach as it allows for the possibility of down-staging the primary tumor in the majority of women thus improving rates of breast preservation [6,7]. Moreover, preoperative therapy also has an additional benefit of assessing the *in vivo* tumor response to a particular drug regimen. Current evaluation of systemic pre-operative therapies relies on post-surgical assessment of removed tissue [8,9], and pathologic complete response (pCR) has been found to be a powerful surrogate of long-term disease-free survival [6–9]. Thus, it is postulated that a therapeutic regimen that produces higher rates of CR in the neoadjuvant chemotherapy (NAC) treatment setting will also provide for higher rates of long-term cure. Ideally, a patient's response to NAC should be detected early and noninvasively using imaging to provide quantitative assessment of treatment responsiveness. As more varied, targeted, and effective systemic therapies are developed, this capability could facilitate the individualization of patient care by providing the opportunity to tailor subsequent treatments for a particular patient based on response to the initial treatment.

DW-MR provides the ability to quantify changes in the Brownian motion of water [10] which is capable of detecting subtle changes in the microenvironment of living tissue. The structure within the microenvironment that affects water diffusivity includes tissue cellularity and extracellular volume, especially when changes are monitored early following treatment initiation. Initial application of diffusion characterization of CNS tumors revealed high apparent diffusion coefficient (ADC) values within necrotic regions of tumors [11–13]. These observations were confirmed in subsequent diffusion studies on both human and animal tumors [14–16]; and recently a correlation between tumor cellularity and ADC was demonstrated in a study of glioma patients [17]. These works suggest diffusion has the potential to aid distinction

of necrotic from viable tumor. Given that diffusion MRI is sensitive to structure at the cellular level, it has the potential to detect and quantify cellular changes that occur in response to successful therapeutic intervention. Moreover, it is reasonable to expect such changes would be measurable prior to macroscopic changes in mass, size, or morphology since removal of debris occurs relatively slowly. The consistent observation of high diffusion in necrotic tissue relative to solid tumor suggests a positive therapeutic effect should register as an increase in diffusion values relative to untreated tumor. Indeed, this has been the pattern observed by several groups using a variety of tumor models and anti-cancer treatments [18–20]. In our experiments with an intracranial rodent glioma model, we observed a 50–100% increase in solid tumor diffusion values following treatment with a chemotherapeutic agent [18–21]. Changes were measurable within two days, peaked within 6–8 days following treatment, and persisted until tumor regrowth shifted ADC back to pretreatment levels. Qualitatively similar findings have been reported using multiple murine tumor models (including breast tumors [22]) and different therapies [18–25]. Results of these studies suggest that quantitative water diffusion measurement/imaging offers potential for early assessment of anti-neoplastic treatment response. Through our own research efforts and those of other laboratories DW-MR is proving to be capable of evaluating treatment response in both preclinical and clinical settings as an early biomarker of subsequent tumor response [26–31]. In preliminary pilot studies, DW-MR was recently reported to show promising results for early response assessment in breast cancer patients [32–35] thus DW-MR appears to offer substantial potential for making substantial inroads into the goal of predicting clinical treatment response early using imaging metrics.

Much of the work to date has involved the use of summary statistics for evaluating therapeutic response using ADC measurements in tumor. Although an increase in water diffusivity as measured by DW-MR has been shown to reflect improved killing of tumor cells [36], spatial heterogeneity in the tumor response to treatment has been shown to attenuate the sensitivity of ADC as determined by whole-tumor statistic (e.g. mean) [37,38]. In a recent study of a population of patients with primary CNS tumors, we prospectively compared tumor ADC at 3 weeks after initiation of therapy with pretreatment images to quantify therapy-induced changes in ADC [37,38]. To account for regional variations in response, two image datasets from before and after treatment were co-registered [39] and analyzed to yield parametric response maps (PRM) as illustrated in Fig 1 [40–42]. These maps present a color overlay of therapeutic induced ADC changes within the tumor, where different regions within the tumor are stratified based on increasing (red), decreasing (blue), or stable (green) ADC values. PRM response metrics were found to correlate better with radiographic response at 10 weeks [36–38,43,44] and overall survival [43] than either histogram measured mean ADC changes or early volumetric changes.

In this study, we obtained DW-MR data from both a single site and from a multi-center prospective clinical trial in which individuals with primary breast cancer treated with NAC were enrolled. To monitor for treatment-induced alterations in tumor cellularity, serial DW-MR scans were acquired at baseline (prior to treatment) and at again at 1–2 time intervals following the start of therapy but before treatment conclusion. Clinical outcomes data was used to assess the utility of PRM, a voxel-based analytical technique and percent change in mean histogram values, as applied to serial ADC maps for their predictive capability as imaging biomarkers for early assessment of clinical treatment response. In addition, a subset of patients from a single-center prospective trial was used to determine the repeatability threshold of ADC measurements by acquiring short interval (<1hr) serial DW-MR examinations to delineate instrumentation noise and ADC measurement variability using a thermally-controlled diffusion phantom [45–47]. We report that ADC measurements can be reliably obtained serially in

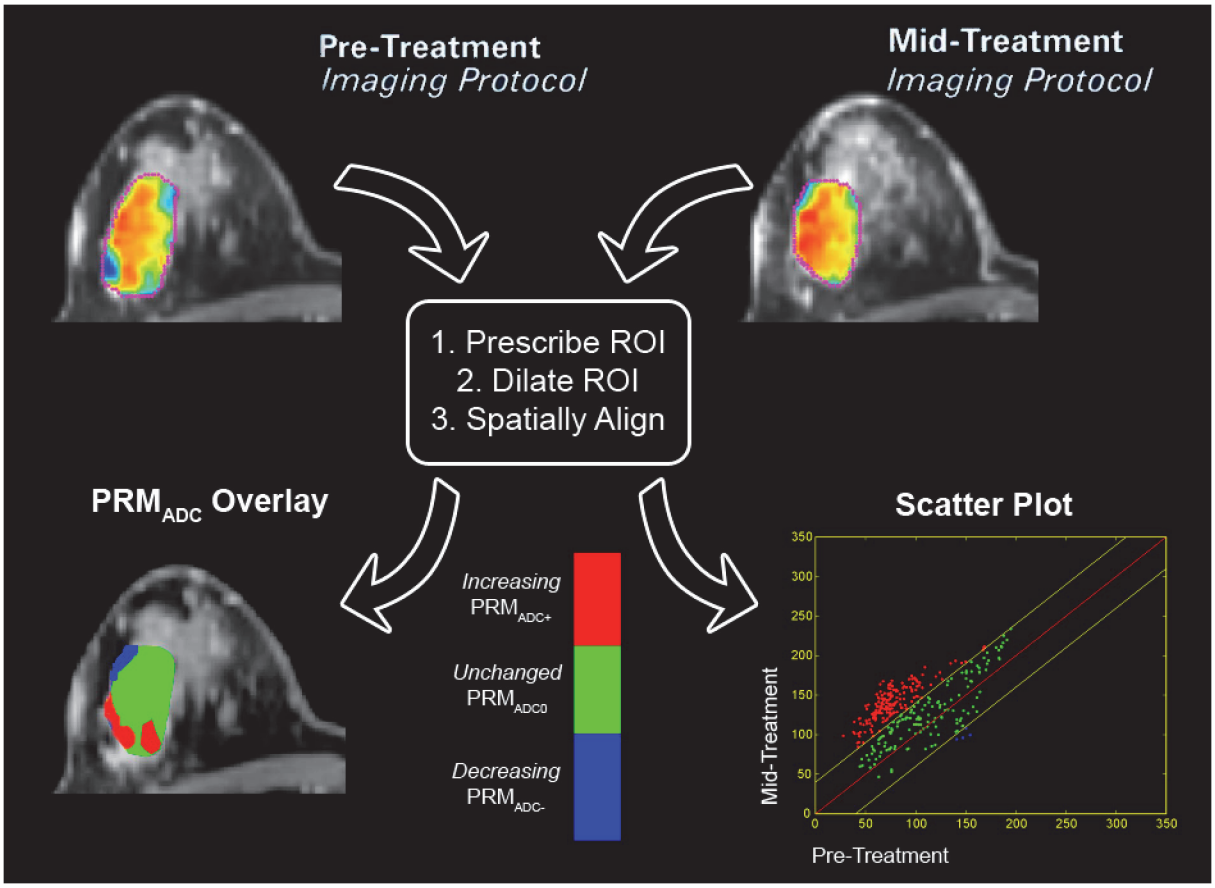

Fig 1. Pictorial representation of the PRM analytical process on ADC maps. Regions of interest (ROI) are prescribed on the pretreatment anatomical images. ROI are then dilated to encompass neighboring tissue around tumor. Control points are automatically distributed throughout the new ROI, where three-five control points must be user defined. Diffusion–weighted MRI data undergoes co-registration to pretreatment anatomical image. Registered pre and mid-treatment ADC maps are used to generate a three-color overlay representing regions in which tumor ADC values significantly increased (red voxels), significantly decreased (blue voxels) or remain unchanged (green voxels). This data can also be presented in a scatter plot and percentages assigned to the three defined ADC regions, allowing quantitative assessment of overall changes in tumor ADC values.

doi:10.1371/journal.pone.0122151.g001

breast cancer patients undergoing NAC and that PRM analysis appears to provide for improved sensitivity over histogram-based mean diffusion changes for early response assessment.

Materials and Methods

University of Michigan (UM)

Ethics Statement. This study was approved by the University of Michigan Institutional Review Board. Subjects with newly diagnosed breast cancer were enrolled on a protocol of intra-treatment MRI (IRB: HUM00003392, Patient Recruitment: 2006–2013). Written informed consent was given by the patients for their information to be used for our research. The University of Michigan clinical trial (UM) consisted of short interval MRI examination, approximately within a 30 minute interval, which were acquired on 13 subjects within 7 days prior to therapy. Eleven of these subjects were used for subsequent analysis as one patient opted out of the study and another was not utilized due to an indeterminate clinical outcome, had an additional MRI examination performed at 8–11 days post-treatment initiation. Treatment consisted of NAC consisting of doxorubicin (60 mg/m^2) plus cyclophosphamide (600 mg/m^2) administered every

2 weeks for a total of four cycles, followed by paclitaxel administered every 2 weeks for an additional four cycles of NAC. Clinical response was assessed by palpation following the conclusion of the first treatment cycle.

MRI scans were performed on a 3T Philips Achieva MRI system (Best, the Netherlands) using a seven-channel phased-array breast coil. Each interval exam included a gadolinium–diethylenetriamine pentaacetic acid (Gd-DTPA; Bayer HealthCare Pharmaceuticals, Wayne, NJ)–enhanced three-dimensional fast field echo T_1-weighted sequence (FOV, 240×240 mm; matrix, 240×240; slice thickness, 1 mm; slices,160; TR/TE/inversion time [TI], 9.9:4.6:1040 milliseconds; turbofactor 200), and a diffusion-weighted (DW), single-shot, spin-echo, echo-planar imaging (EPI) series (FOV, 270×270 mm; matrix, 205×205; slice thickness, 4 mm; slices, 24; TR/TE, 2789/59 milliseconds; b factor 0 and 800 sec/mm^2) with diffusion sensitization along three orthogonal directions. DWI was acquired prior to Gd-DTPA administration. All images were acquired with a SENSitivity Encoding (SENSE) acquisition scheme [22]. The SENSE factor for all images was 2, except diffusion scans which had a SENSE factor of 3.9. The total duration of this acquisition protocol (including patient setup) was approximately 35 to 60 minutes, with DW-MR scans requiring approximately 2 minutes of scan time.

University of Hull, England and NeoCOMICE

Courtesy of the University of Hull, UK was a single-site study (Hull) consisting of 27 de-identified image data sets with clinical outcomes provided, of which 13 were used in this study. An additional 26, of which 14 were used, were provided from the Cancer Research UK funded multisite UK clinical trial NeoCOMICE (UKCRN ID 5828) ISRCTN42613663. Both the University of Hull and NeoCOMICE had IRB approvals from their respective institutions for these trials. Written informed consent was given by the patients for their information to be used for our research. All data received by UM from Hull and NeoCOMICE was anonymized and de-identified prior to arrival. The remaining datasets were excluded from the study due to incomplete scans, missing first or second post-treatment data, no outcome results or extensive image artifacts. For both datasets subjects were enrolled who were newly diagnosed with breast cancer. Treatment primarily consisted of epirubicin (90 mg/m^2) and cyclophosphamide (600 mg/m^2) administered at 3 week intervals. MR scans were performed approximately 8 days prior to treatment and 7 days and again 35 days post-treatment initiation. Therapeutic outcomes were determined using RECIST 1.1 response criteria from assessment of tumor volumetric changes in MR images from pretreatment to the time of therapy completion [48].

MRI scans were performed on both 1.5T and 3.0T MRI systems utilizing dedicated bilateral breast coils [49]. Each interval exam included Gd-DTPA-enhanced T_1-weighted sequence (parameters) and a DW, single-shot, dual spin-echo, EPI sequence acquired axially with a water-only excitation (TR/TE, 4000/74 ms (3.0 T) or 4000/98 ms (1.5 T); FOV, 340×340 mm; matrix, 128×128; slice, 5 mm; gap, 1 mm; 10 averages; one b_0 acquisition, and three b = 700 s/mm^2 acquisitions applied in orthogonal directions. DW-MR scans were acquired in 2 min 40 sec.

Thermally-Controlled Diffusion Phantom

We employed a thermally-controlled diffusion phantom, developed by our group, to assess the repeatability of ADC measurements and the impact of instrumentation noise to these measurements. The phantom used in this study has been previously described [45,50]. Briefly, the phantom consisted of 50 mL polypropylene conical tube inserted in a 1000 mL polypropylene wide-mouth jar. The 50 mL tube was filled with distilled water and placed in the 1000 mL jar which was filled with crushed ice and water. The water within the tube equilibrated to 0°C within 30 minutes of insertion into the jar. DW images were acquired on a 3T Philips using a

8-channel head coil using a single-shot, spin-echo, echo-planar imaging (EPI) series (FOV, 270×270 mm; matrix, 205×205; slice thickness, 4 mm; slices, 24; TR/TE, 2789/59 milliseconds; b factor 0 and 800 sec/mm^2) with diffusion sensitization along three orthogonal directions.

Image Analysis

All MRI data were transferred to a PC, interpolated to a matrix of 256x256, and analyzed using in-house software developed in MATLAB (The MathWorks, Inc., Natick, MA). The product of the three orthogonal DW-MR images exhibits strong sensitivity to diffusion with no dependence on structural directionality in the tissues. This isotropic feature was crucial for following serial changes in water diffusivity, quantified as the apparent diffusion coefficient (ADC), without confounding effects due to tissue orientation. ADC maps were calculated using the following equation:

$$\mathrm{ADC} = \ln \frac{S_{b_0}}{S_{b_{800}}} / (b_{800} - b_0) \quad (1)$$

where S_{b_0} and $S_{b_{800}}$ are the signal intensities acquired at low and high diffusion sensitivity, respectively, b_0 and b_{800} are the low and high b-values in units of s/mm^2, respectively, and ADC is the apparent diffusion coefficient obtained using b_0 and b_{800}. Subsequent to image registration, contours were manually drawn by a MRI breast radiologist over tumors as delineated on contrast-enhanced T_1-weighted images. From the region-of-interest (ROI) tumor volume and mean ADC were assessed at each interval exam.

Parametric Response Map (PRM)

Presented in Fig 1 is a schematic representation of PRM work flow. Image registration of the mid-treatment ADC map (homologous image) to the pre-treatment ADC map (reference image) was performed first using a rigid body registration to account for spatial repositioning. As a consequence of the soft breast tissue large deformation may occur during serial examinations. A deformable algorithm that employed thin plate splines was used to account for deformation of the breast tumor [51]. To minimize processing time while increasing accuracy of the deformable registration process, image alignment was performed only on the prescribed ROI. For both rigid and deformable registration mutual information was used as an objective function and simplex as an optimizer [39,52]. Approximately 30 equidistant control points were automatically positioned within the reference image, where 5 of these points were manually selected. The remaining control points were automatically aligned, resulting in an approximate 10 minutes of computational time. Subsequent to image registration, individual voxels, the smallest unit of volume, were classified based on the extent of change in the ADC value. This was performed by calculating the difference between ADC values (ΔADC = mid-treatment ADC–pre-treatment ADC) for each voxel within the tumor ROI. Voxels yielding ΔADC greater than a predetermined threshold of $0.45\text{x}10^{-3}$mm^2/s (described below) were coded red (i.e. Red: $\Delta\mathrm{ADC} > 0.45\text{x}10^{-3}$mm^2/s), voxels with values less than $-0.45\text{x}10^{-3}$mm^2/s were coded blue (i.e. Blue: $\Delta\mathrm{ADC} < 0.45\text{x}10^{-3}$mm^2/s), and all other voxels were coded green (i.e. Green: $-0.45\text{x}10^{-3}\text{mm}^2/\text{s} \leq \Delta\mathrm{ADC} \leq 0.45\text{x}10^{-3}\text{mm}^2/\text{s}$). Global PRM measures were calculated by normalizing the sum of all voxels within a classification by the total tumor volume. The nomenclature of these measures are $\mathrm{PRM}_{\mathrm{ADC+}}$ for the relative tumor volume with increasing ADC, $\mathrm{PRM}_{\mathrm{ADC-}}$ for the relative tumor volume with decreasing ADC, and $\mathrm{PRM}_{\mathrm{ADC0}}$ for the relative tumor volume with unchanged ADC.

We empirically calculated the thresholds that designate a significant change in ADC within a voxel from the 13 subjects who underwent pre-treatment serial MRI examination within a short time interval (~30 minutes between examinations). For each subject, tumors were manually

contoured and spatially aligned as described above such that each tumor voxel consisted of an ADC pair. We then determined the 95% confidence intervals (CI) from the resulting linear least-squares fit of the joint density histogram (illustrated in Fig 1). The mean of all 95% CIs was used as the PRM threshold for therapeutic response assessment of the multisite data.

Data and Statistical Analysis

To illustrate the importance of image registration to account for spatial heterogeneity in a tumor volume we determined the 95% confidence interval of tumor ADC differences for each subject. Short interval ADC measurements, "test-retest", were evaluated by calculating the mean and the standard deviation of ADC values over the entire tumor volume for each subject. As an approximation, the error associated with the difference in the serial mean ADC values was determined by propagation of error, $\sigma_{\Delta}^{2} = \sigma_{A}^{2} + \sigma_{B}^{2}$ where σ is the standard deviation and A, B and Δ indicate the first examination, second examination and difference between examinations, respectively. The 0.975 quantile of the difference in mean ADC values within a subject tumor was then determined by the following expression, 1.96xstandard deviation. Differences in age and initial tumor volume between accrual sites were determined using an unpaired 2-tailed Student's t-test. Differences in tumor grade between sites were determined using a Likelihood Ratio test. Due to the relatively small number of subjects in each of the studies, patient's designated complete response (CR) and partial response (PR) were pooled into a single classifier called responders and stable disease (SD) and progressive disease (PD) patients were classified as non-responders. The percent change in mean ADC and PRM measures were assessed between responders and non-responders by an unpaired 2-tailed Student's t-test at time points 3–5 days, 8–11 days and 35 days. Finally, receiver operating characteristic (ROC) curve analysis was performed to determine the predictive potential of the percentage change in ADC and PRM parameters with subject clinical response. Data are presented as mean±SEM, unless stated otherwise. All statistical computations were performed using a statistical software package (IBM SPSS Statistics, Armonk, NY), and declared statistically significant at the two-sided 5% comparison-wise significance level ($p < 0.05$).

The raw data used in the final analyses has been provided as a table (S1 Table). This table contains anonymized numerical summary statistics, at the individual voxel and subject level of ADC and delta-ADC values from within the tumor ROIs for each subject/time point. Furthermore, while informed consent and HIPA regulations apply to this clinical trial data set which places limits on providing the original image data, interested parties seeking to access the original image data should contact the communicating author to discuss and complete the required institutional Material Transfer Agreement documentation.

Results and Discussion

Test-Retest

To determine variations in ADC measurements associated with instrumentation noise as well as provide a means of establishing thresholds for the PRM approach, MRI examinations were obtained in short intervals on 13 breast cancer patients accrued at the UM. Fig 2A demonstrates the test-retest results for these 13 subjects. Mean values in tumor ADC were bounded between 0.5 and $1.5x10^{-3}mm^2/s$ with standard deviations observed as high as $0.6x10^{-3}mm^2/s$. In a comparative study, we performed a repeatability experiment where on 16 separate occasions ADC measurements were acquired from a thermal-controlled diffusion phantom that consisted of liquid water at near freezing temperature [45,50]. Here, ADC values were consistently measured around the literature value of $1.1x10^{-3}mm^2/s$ [53] with the mean in the standard deviations at $0.02x10^{-3}mm^2/s$ (Fig 2B). As this was a homogeneous water phantom, the

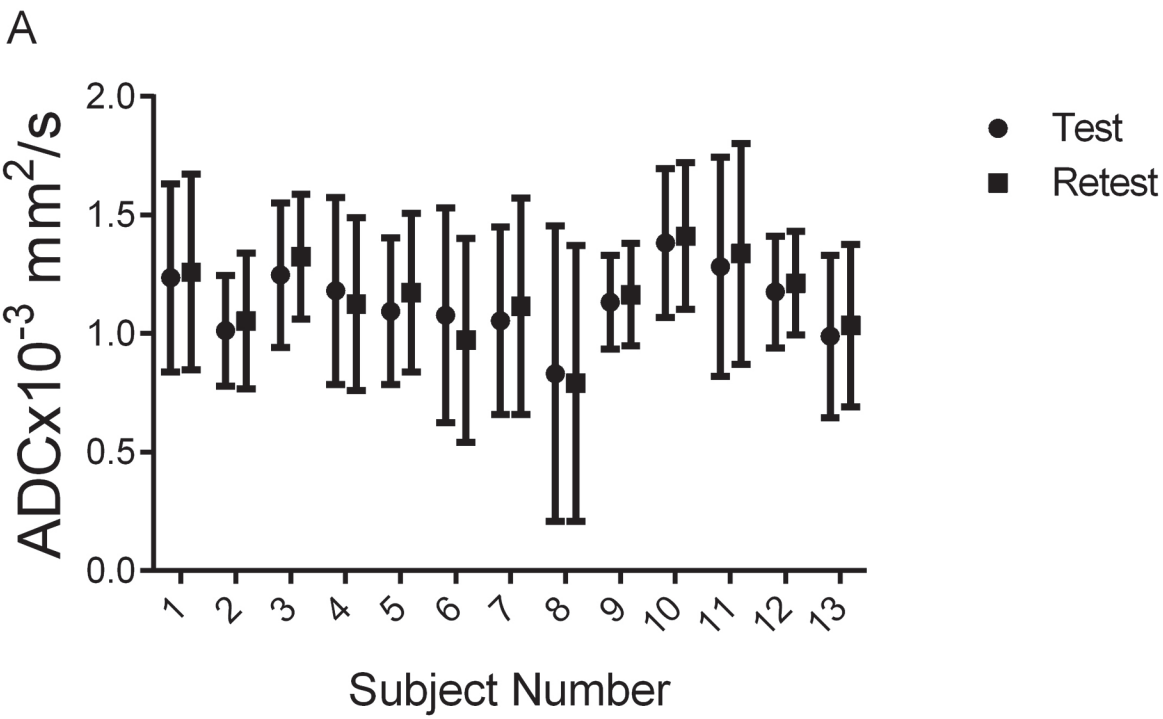

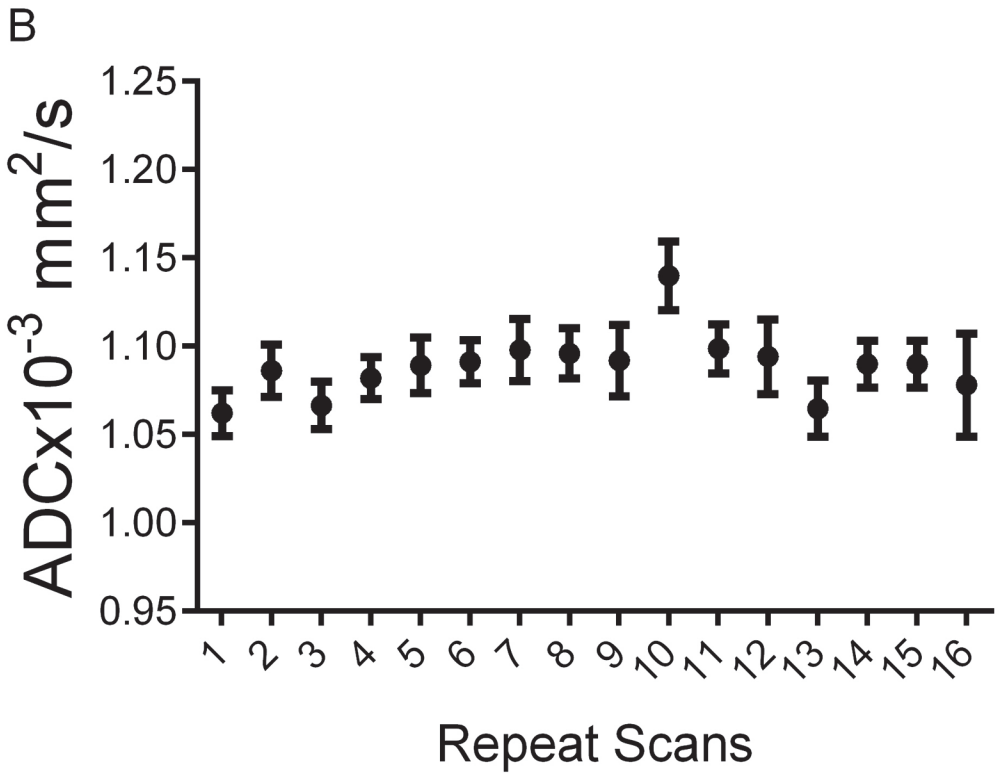

Fig 2. ADC Results from test-retest human breast and phantom studies. Presented are summary plots of mean ADC values from (A) the test-retest of breast tumors from individual subjects accrued at the UM and (B) the repeatability analysis using a thermal-controlled diffusion phantom (i.e. ice water phantom [45,50]). Data is presented as the mean±standard deviation.

doi:10.1371/journal.pone.0122151.g002

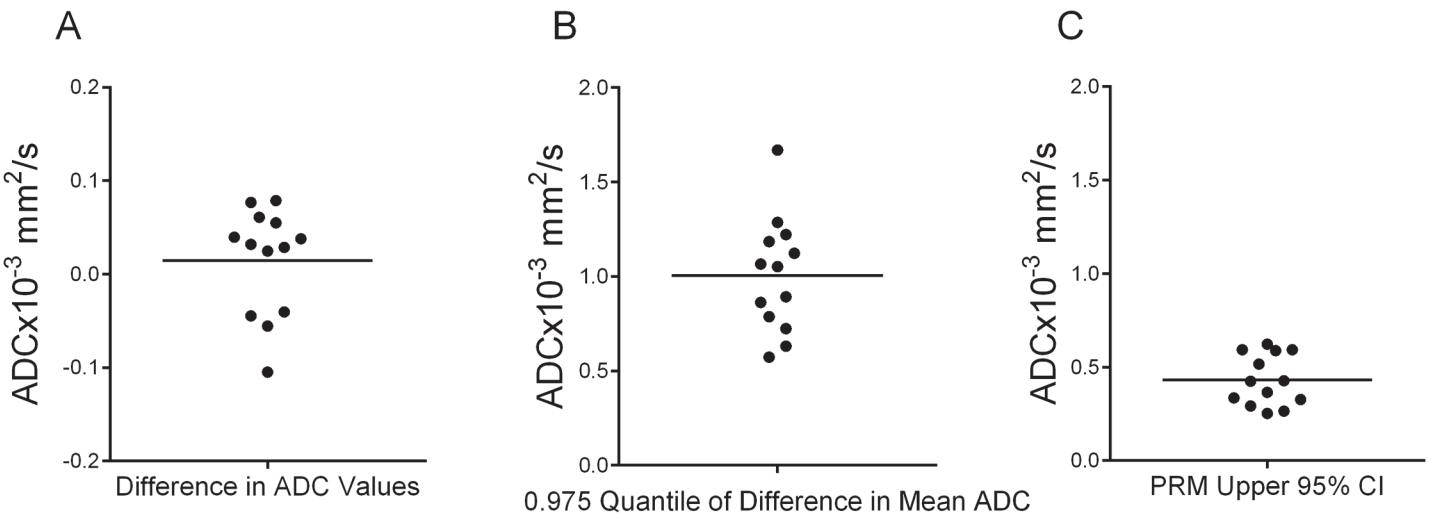

Fig 3. Evaluation of ADC variability in test-retest data. Presented are scatter plots of (A) the difference in mean ADC tumor values, (B) the 0.975 quantile of the difference in mean ADC tumor values, and (C) the PRM 95% CI generated from the fit of the joint density histogram of voxels from spatially aligned serial ADC tumor maps. The 0.975 quantile of the difference in mean ADC values was determined by propagating the error (standard deviation) and calculating the 0.975 quantile as 1.96xstandard deviation. Each dot represents a single patient and the large line the mean of the entire group.

doi:10.1371/journal.pone.0122151.g003

observed standard deviations in the ADC measurements are directly attributed to instrumentation noise. We postulate that the large discrepancy in the standard deviations of the ADC values between the breast tumors and phantom was attributed almost entirely by tumor heterogeneity.

As seen in Fig 3A, the difference in the mean ADC tumor values between serial examinations varied by less than $\pm 0.1 \times 10^{-3} mm^2/s$. By propagating the error, we acquired an estimate of the 0.975 quantile of the difference in the mean ADC tumor values for each subject. Here we found the mean 0.975 quantile was about $1 \times 10^{-3} mm^2/s$ for all subjects, again attributed mostly to large variations in tumor tissue rather than instrumentation noise (Fig 3B). The 95% confidence interval obtained from the linear least-squares fit of the joint density histogram of spatially aligned serial ADC maps (illustrated in Fig 1) was found to be approximately half (mean value of $0.45 \times 10^{-3} mm^2/s$ with a range of 0.25 to $0.62 \times 10^{-3} mm^2/s$) of what was observed by simply propagating the error from the whole-tumor estimates. In the absence of any physiological changes in the tumor that may adversely affect tumor ADC, only instrumentation noise would cause variability in the ADC measurement from serial maps perfectly aligned. As this is not the case, slight imperfections in the image registration have occurred. Nevertheless, the value determined from the joint density histogram is consistent with previously published results [38,54,55]. All subsequent PRM analyses were performed using this determined value (i.e. $\pm 0.45 \times 10^{-3} mm^2/s$).

Subject Characteristics

Thirty-nine subjects with newly diagnosed primary breast cancer were included in this analysis, accrued as part of three separate clinical trials: 11 from UM, 13 from Hull and 14 from the multicenter UK trial NeoCOMICE. A summary of patient characteristics is provided in Table 1. All subjects underwent NAC for multiple cycles following their own respect treatment regimen. Controlling for multiple comparisons, Hull subjects were found to be significantly older in age than UM subjects ($p = 0.003$). Although there was some disparity in patient age, there were no significant differences in tum or grade or initial tumor volume between accrual sites.

Table 1. Patient Characteristics.

ID	Site	Age	Type	Initial Tumor Volume (cm3)	Grade	Outcome
1	UM	59	ductal	10.9	3	PR
2	UM	48	ductal (apocrine)	3.2	3	PR
3	UM	47	ductal	25.8	2	PR
4	UM	41	ductal (apocrine)	12.2	2	SD
5	UM	24	ductal	11.6	3	CR
6	UM	64	ductal	5	3	PR
7	UM	41	ductal	13.3	2	SD
8	UM	41	ductal	4.2	3	CR
9	UM	43	ductal	12.8	2	SD
10	UM	37	ductal	1.6	1	PR
11	UM	46	ductal	4.4	3	PD
12	Hull	51	NST	15.7	2	SD
13	Hull	66	NST	5.5	3	PR
14	Hull	54	Ductal	16.9	3	PR
15	Hull	62	NST	28	3	PR
16	Hull	69	NST	4.3	3	PR
17	Hull	53	Ductal	20.5	3	PR
18	Hull	55	Ductal	18.3	3	SD
19	Hull	53	Ductal	61	2	PR
20	Hull	46	NST	54.8	3	PR
21	Hull	57	Ductal	36.8	2	PR
22	Hull	58	NST	6.3	3	SD
23	Hull	65	Mucinous	12.1	2	PR
24	Hull	59	Ductal	11.5	2	PR
25	NeoComice	41	Ductal/no special type	166.6	2	SD
26	NeoComice	63	Ductal/no special type	21.5	3	PD
27	NeoComice	62	Ductal/no special type	5.6	3	SD
28	NeoComice	62	Ductal/no special type	9.8	3	PR
29	NeoComice	47	Ductal/no special type	14.6	2	SD
30	NeoComice	48	Ductal/no special type	8	2	SD
31	NeoComice	48	lobular	181	2	SD
32	NeoComice	50	Ductal/no special type	4.6	3	SD
33	NeoComice	34	Ductal/no special type	7.2	3	SD
34	NeoComice	44	Ductal/no special type	27.4	2	SD
35	NeoComice	56	Ductal/no special type	35.7	3	SD
36	NeoComice	53	lobular	11.2	2	PR
37	NeoComice	57	Ductal/no special type	9.9	2	PD
38	NeoComice	39	Ductal/no special type	45.2	3	PR

Note: Outcomes are based on RECIST with the convention: CR for complete response, PR for partial response, SD for stable disease and PD for progressive disease.

doi:10.1371/journal.pone.0122151.t001

Therapeutic Response by DW-MRI

Contrast-enhancing images and ADC maps pre and mid-treatment are presented for UM accrued patients identified by palpation following one cycle of treatment as SD and CR (Fig 4 top and bottom rows, respectively). The representative ADC maps pre-treatment clearly identify the heterogeneous distribution of ADC values throughout the tumor (Fig 4B and 4F).

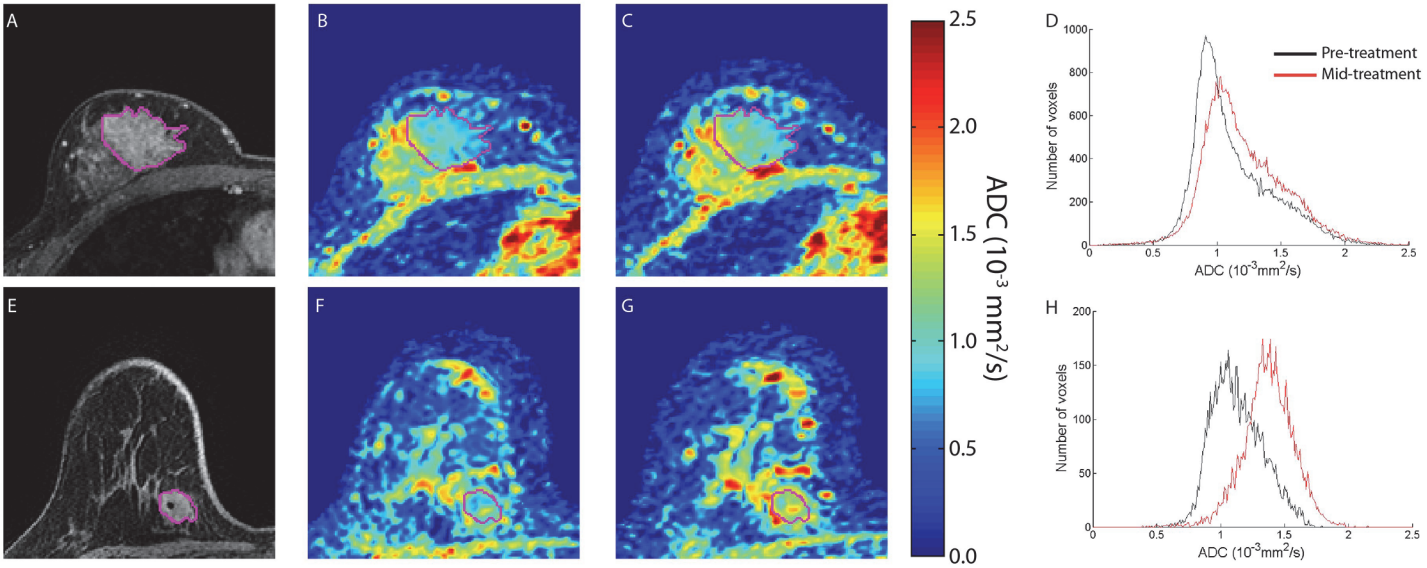

Fig 4. Therapeutic-induced changes in breast tumor ADC values. MRI images are depicted for non-responding (top row) and responding (bottom row) patients treated for breast cancer. (A) and (E) T1-weighted gadolinium enhanced, (B) and (F): pre-treatment ADC maps, (C) and (G): ADC maps at 8–11 days after treatment initiation, D) and (H): Histograms of ADC values in the tumor pre-treatment and post-treatment initiation. Tumor is delineated from surrounding healthy tissue in the individual images by the purple line.

doi:10.1371/journal.pone.0122151.g004

Following a therapeutic intervention, a negligible change in the tumor ADC at serial time points was observed in the patient with the stable disease. Mean ADC values were found to be $1.1x10^{-3}$ mm^2/s and $1.2x10^{-3}$ mm^2/s pre and mid-treatment, respectively, resulting in a percent change in ADC of 8% (Fig 4D). Only a 6% decrease in tumor volume was observed in the SD patient. For the CR patient, the histogram of the mid-treatment ADC values, as seen in Fig 4, shifted to higher ADC values. In fact, mean ADC increased by 21% from $1.1x10^{-3}$ mm^2/s and $1.4x10^{-3}$ mm^2/s pre and mid-treatment, respectively (Fig 4H), whereas the tumor volume had only decreased by 2%.

Application of the PRM technique on serial ADC maps identified substantially less tumor volume with increasing ADC values mid-treatment in the SD patient as compared to the CR patient (Fig 5). For the SD patient, only 1.8% of the tumor volume was found to generate increasing ADC values that were beyond the 95% confidence interval ($\pm 0.45x10^{-3}$mm^2/s). This suggests that a large segment of the tumor volume was unresponsive to the therapeutic intervention. For the CR patient, up to 12.8% of the tumor was designated by PRM as demonstrating an increase in ADC beyond the $0.45x10^{-3}$mm^2/s threshold. Responsive tissue within the tumor is clearly identified with the PRM_{ADC} map as red voxels, suggestive of a reduction in tumor cellularity in response to an effective therapy. Increasing values in PRM_{ADC+} has been shown to correlate with cell kill in preclinical models of brain tumors and metastatic cancer to the bone [27,36].

MRI examination time intervals varied between sites. As such, we evaluated PRM and percent change in ADC from histogram analysis at 3–5 days (Hull and NeoCOMICE), 8–11 days (UM) and 35 days (Hull and NeoCOMICE) post-treatment initiation along with ROC analysis of several individual imaging-based biomarker metrics (Fig 6). For the analysis, the response groups were pooled such that CR and PR were classified as responders and SD and PD were classified as non-responders. Percentage change determined from ADC histogram analysis was not significant for patients classified as responders versus non-responders at either the 3–5 day interval (10.6±4.5% and 3.3±2.2%) or the 8–11 day interval (9.1±2.7% and 4.7±3.1%) (Fig 6A).

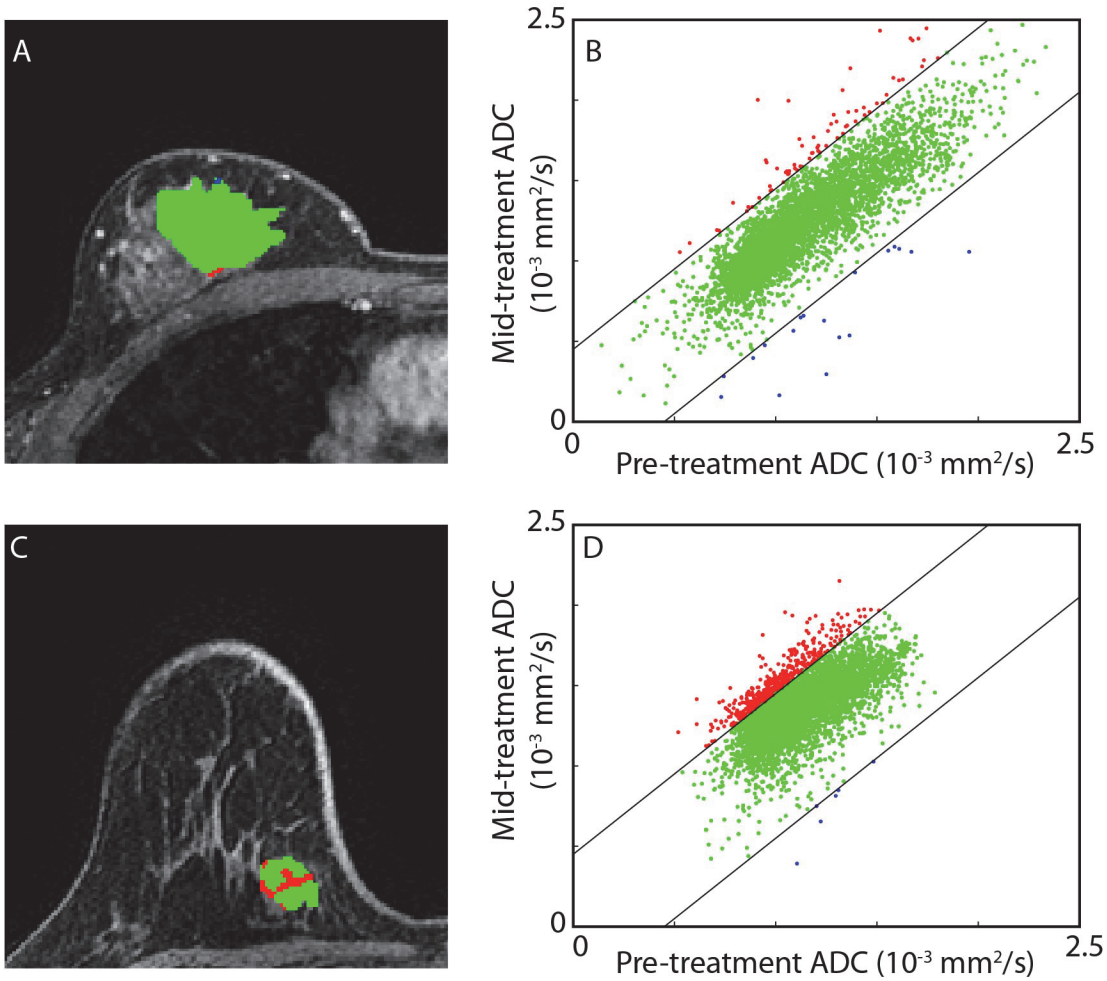

Fig 5. Evaluation of PRM_{ADC} as a response metric. Parametric response maps (A) and (C) and corresponding scatter plots (B) and (D) of post- versus pre-treatment ADC values are presented for a representative non-responder (top row) and responder (bottom row). The joint density histogram from the non-responder demonstrated a negligible shift resulting in a PRM_{ADC+}, i.e., the relative tumor volume with significantly increasing ADC values, of 1.8%. In contrast, a substantial shift in the histogram was observed for the responder (PRM_{ADC+} of 12.8%).

doi:10.1371/journal.pone.0122151.g005

However, the percent change in the mean tumor ADC was found to be significantly higher in responders at 35 days post-treatment initiation versus non-responders (11.3±2.5% for responders and 0.3±2.9% for non-responders, p = 0.012) (Fig 6D). PRM_{ADC-} produced no significant difference between responders and non-responders at 3–5 days (3.2±0.6% and 3.5±1.2%), 8–11 days (3.8±1.4% and 2.1±1.6%) and 35 days (6.6±2.1% and 8.8±3.4%). PRM_{ADC+} at 3–5 days was similar between groups (8.3±1.9% for responders and 8.6±3.2% for non-responders). Differences in the PRM_{ADC+} metric became evident at as early as the 8–11 day examination time point (8.4±0.9% for responders and 2.2±1.2% for non-responders; p = 0.006) with responders (Fig 6B). Furthermore, PRM_{ADC+} was also found to be predictive of response at the 35 day interval with responders having a PRM_{ADC+} of 17.4±2.8% which was significantly higher in value from the PRM_{ADC+} of the non-responder group (7/4±1.5%, p = 0.004) (Fig 6E). For the 8–11 day data, ROC analysis revealed an AUC value of 0.964 (p = 0.01) versus 0.714 (p = 0.26) for PRM_{ADC+} and percent change in mean histogram ADC, respectively. For the 35 day data, ROC analysis revealed an AUC value of 0.770 (p = 0.05) versus 0.825 (p = 0.02) for PRM_{ADC+} and percent change in mean histogram ADC, respectively.

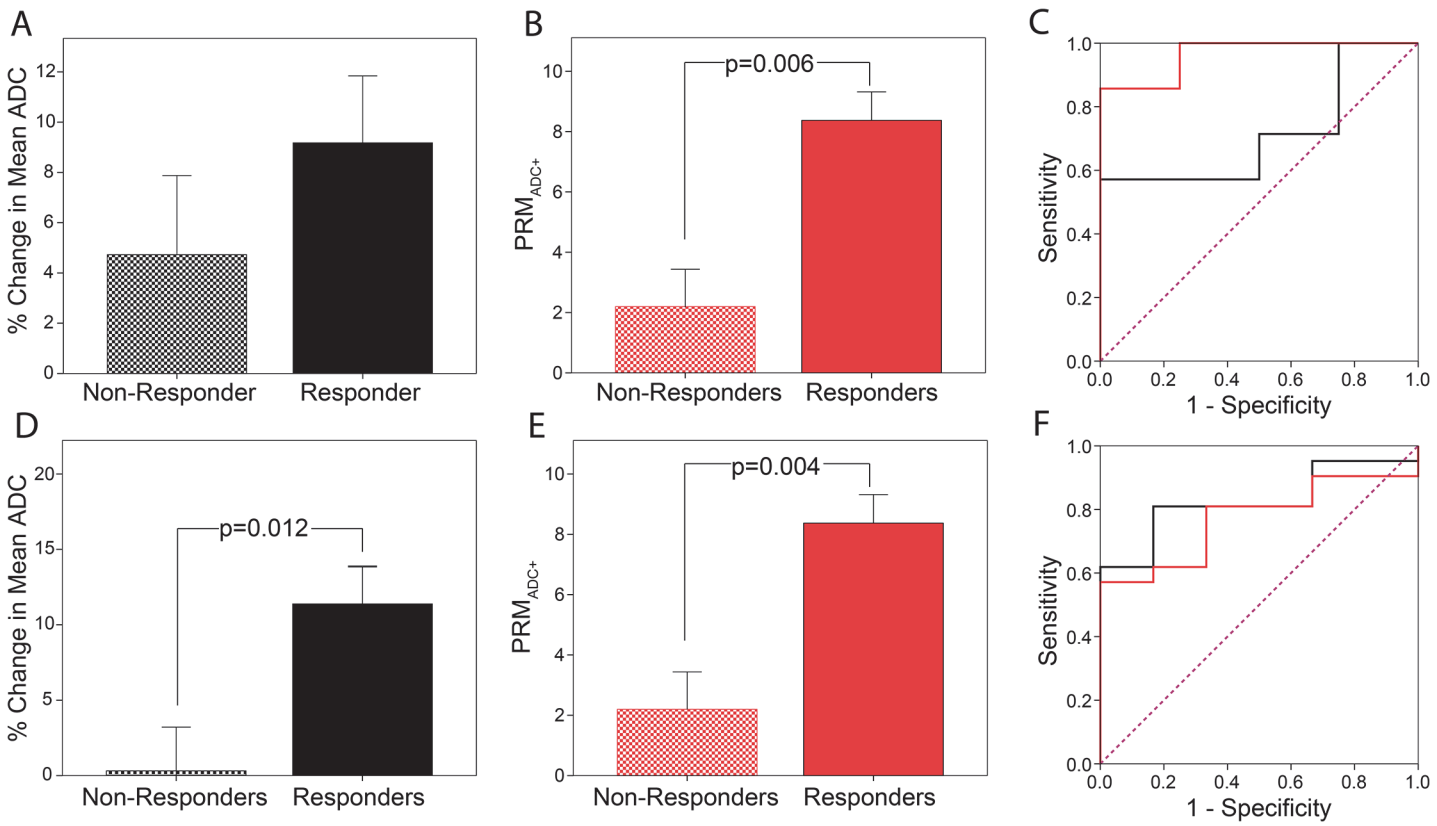

Fig 6. DW-MRI results at interval MRI examinations. Presented are results from MRI data acquired at (A-C) UM (8–11 days) and (D-F) NeoCOMICE (35 days). The analyses include the percent change in mean ADC values and (B, E) PRM values of cancer patients diagnosed as responders and non-responders at three different interval MRI examinations as well as (C,F) ROC analysis for both readouts. Statistical significance was assessed at $p<0.05$. Data acquired at 8–11 days was obtained at the University of Michigan, where other interval data was acquired as part of a UK clinical trial.

doi:10.1371/journal.pone.0122151.g006

NAC is used as a standard treatment to improve surgical outcomes for patients with inoperable locally advanced breast cancer, and to improve breast conservation rates in patients with operable breast cancer. For such an approach to be optimally employed an accurate surrogate biomarker of therapeutic tumor response must be developed to identify patients unresponsive to NAC. DW-MR is one such imaging technique that has shown great promise at detecting tumor therapeutic response. A standard sequence on most MRI systems, DW-MR has found widespread use for diagnostic and prognostic application in the medical community [40,44,56,57]. The appeal of this technique is its high sensitivity to microenvironmental changes in living tissue that commonly occurs upon the onset or treatment of disease [58,59]. In addition, this MRI technique is inherently noninvasive, requiring no contrast administration. Preclinical work by our group and others as well as clinical studies have demonstrated the sensitivity of DW-MR for assessing early therapeutic response in breast cancer [26,27,35,36,60,61]. Recent advances in an analytical technique referred to as PRM has shown to improve the sensitivity of quantitative maps (i.e. ADC) at detecting even subtle therapy-induced changes within tumors [27,36–38,43,54,62–64]. In this study, ADC, the functional metric, was evaluated as a surrogate imaging biomarker using conventional summary statistical analysis and a voxel-based (PRM) approach for tumor response to NAC using subject data acquired from multiple clinical sites.

Through collaborative efforts of the Quantitative Imaging Network (http://imaging.cancer.gov/programsandresources/specializedinitiatives/qin) the reproducibility of DW-MR was

evaluated by developing a thermal-controlled diffusion phantom as well as established clinical protocols for proper execution of the DW-MRI examination (ice water phantom and white papers) [52,57]. To date, therapeutic response using ADC measurements continues to be determined primarily using histogram derived whole-tumor summary statistics, where the mean of the ADC values are evaluated serially with disregard for any spatial dependence of the ADC measurements. In this study we observed that the mean ADC tumor values showed negligible variability between short interval serial examinations with $|\Delta ADC| < 0.1x10^{-3}mm^2/s$. This is consistent with the deviation in ADC measurements observed from our repeatability analysis using our phantom where ADC values were typically between $1.05x10^{-3}mm^2/s$ and $1.1x10^{-3}mm^2/s$. In contrast, ADC voxel values within the tumors showed substantially broad distributions, with standard deviations as large as $0.5x10^{-3}mm^2/s$ (Fig 2A and 4D). This is in contrast to our observations from the phantom study. ADC variability in the tumor tissue is attributed to the dependence of ADC voxel values to local microenvironments within the tumor (i.e. tumor cellularity, necrosis, edema and vasculature), which is unlike the homogeneous phantom that exhibits no spatial dependence in ADC. By propagating this error (i.e. standard deviation) we determined that the mean 95% CI of our serial ADC measurements (ΔADC) was approximately $\pm 1x10^{-3}mm^2/s$, with one subject generating a 95% CI as high as $\pm 1.7x10^{-3}mm^2/s$. It is this spatial variability, confounded with spatial variability in tumor response where local ADC simultaneously increases and decreases that attenuates the sensitivity of the whole-tumor statistical ADC measure. By way of spatial alignment of the serial ADC maps we are able to remove much of the variability in the data. Following this procedure, a step in our PRM method, we generated a mean 95% CI of $\pm 0.45x10^{-3}mm^2/s$ (Fig 3C) which is significantly lower than the error observed in Fig 3B ($p<0.0001$ paired t-test).

We applied the PRM approach to serial ADC measurements from three separate prospective clinical trials to assess the sensitivity of PRM_{ADC} as a response metric to NAC in primary breast cancer patients. Our previous work and the work of others using various tumor types, both clinical and preclinical, have identified the relative volume of tumor that demonstrates a significant increase in ADC (PRM_{ADC+}) as the most predictive of response [36–38,40,43,54]. Consistent with these findings we observed at the 35 day interval responders having significantly higher PRM_{ADC+} than non-responders (Fig 6B). Based on the literature where ADC values have been found to inversely correlate strongly with tumor cellularity, the results generated by our PRM method would in fact be in agreement with the "state" of the tumor. Recently, investigators have shown that voxel-based analysis of breast cancer DW-MRI along with dynamic contrast enhanced MR (DCE-MR) images can be used to provide spatial information related to response along with optimization of prognostic accuracy [65] furthering the concept that PRM improves diagnostic accuracy over whole-tumor histogram statistics [42].

There are some limitations in the current study that must be addressed. Test-retest data acquired from our subject population and the diffusion phantom were acquired using different MRI coils. Variations in coil designs may affect signal sensitivity and homogeneity, effecting noise levels in the ADC measurement. Also, if lesion location in the magnet bore relative to iso-center varied between the scans, then gradient nonlinearity may further increase variance. Nevertheless, this analysis illuminates the impact of tumor heterogeneity on quantitative ADC values as determined by DW-MRI. In addition, the repeatability analysis did not account for variations between centers and MRI platforms as all data was acquired at a single site on a single scanner. However, this analysis provides an indication of the robustness and variability of ADC measurements in this cohort of breast cancer subjects. Differences in study design, which include DW-MR sequence parameters examinations times, may have also resulted in an increase in the variability in the ADC measurements. Although pooling the data at the earlier time intervals was an option, due to differences in the study protocols we elected to treat the UM data independently from data acquired at Hull and NeoCOMICE. In contrast, both Hull

and NeoCOMICE were pooled as the study designs were the same for these trials. Consequent to evaluating the data at their interval examination, patient numbers were relatively low. As such the predictive potential of the PRM method may be affected by type I error (false positive) and type II error (false negative). This is also confounded by differences in outcome measures between sites where UM used palpation, Hull and NeoCOMICE used RECIST 1.1. Nevertheless, the results presented in this study provide valuable information on the extent of variability in the ADC measurement and the ability of PRM to be used in multi-center imaging trials.

Conclusion

Our findings support further development of ADC measurements with PRM analysis as a biomarker of early therapeutic response assessment of breast cancer patients undergoing NAC. The study also demonstrated the feasibility of performing a multi-site prospective analysis of DW-MRI as a predictive biomarker of NAC in breast cancer patients. In addition, we provide experimental results supporting the need for more sensitive analytical tools for evaluating ADC measurements such as PRM which also provides for spatial changes to be mapped versus histogram-based metrics. Future studies involving multi-center prospective clinical trials will require adequate quality assurance controls for uniformity in DW-MR sequences as well as consistent ADC measurements through the use of diffusion phantoms to qualify individual MR systems for conducting DW-MR scans. Moreover, multi-modal imaging metrics including hemodynamic information along with DW-MR metrics may add additional prognostic accuracy as was recently reported in a 28 patient NAC trial [34]. Overall, this study has provided approaches which can be implemented to ensure more unified and consistent data collection for improving cross comparison of DW-MR results between clinical sites. Overall, the results presented support the emerging role of DW-MR in the context of early treatment response assessment for breast cancer patients undergoing NAC but a larger multi-center prospective study is needed to confirm these findings.

Supporting Information

S1 Table. Summary of ADC and fDM imaging metrics for all subjects analyzed.
(DOCX)

Author Contributions

Conceived and designed the experiments: LWT AFS NMH BDR TLC TDJ. Performed the experiments: CJG DM MDP NLH AFS CHN NMH TLC LWT. Analyzed the data: CJG BM DM MDP KH NLH AFS CHN NMH AR CRM TLC LWT BDR TDJ. Contributed reagents/materials/analysis tools: CJG BM DM MDP KH NMH AR CRM TLC LWT BDR TDJ. Wrote the paper: CJG BM DM MDP KH NLH AFS CHN NMH AR CRM TLC LWT BDR TDJ.

References

1. Baum M. Polychemotherapy for early breast cancer. Lancet. 1998; 352: 1554. PMID: 9820332
2. Saibara T, Ogawa Y, Onishi S. Tamoxifen in early breast cancer. Lancet. 1998; 352: 404. PMID: 9717955
3. Buzdar AU, Ibrahim NK, Francis D, Booser DJ, Thomas ES, Theriault RL, et al. Significantly higher pathologic complete remission rate after neoadjuvant therapy with trastuzumab, paclitaxel, and epirubicin chemotherapy: results of a randomized trial in human epidermal growth factor receptor 2-positive operable breast cancer. J Clin Oncol. 2005; 23: 3676–3685. PMID: 15738535
4. Romond EH, Perez EA, Bryant J, Suman VJ, Geyer CE Jr., Davidson NE, et al. Trastuzumab plus adjuvant chemotherapy for operable HER2-positive breast cancer. N Engl J Med. 2005; 353: 1673–1684. PMID: 16236738

5. Valero V, Buzdar AU, McNeese M, Singletary E, Hortobagyi GN. Primary chemotherapy in the treatment of breast cancer: the University of Texas M. D. Anderson Cancer Center experience. Clin Breast Cancer. 2002; 3 Suppl 2: 63–68.
6. Fisher B, Brown A, Mamounas E, Wieand S, Robidoux A, Margolese RG, et al. Effect of preoperative chemotherapy on local-regional disease in women with operable breast cancer: findings from National Surgical Adjuvant Breast and Bowel Project B-18. J Clin Oncol. 1997; 15: 2483–2493. PMID: 9215816
7. Newman LA, Buzdar AU, Singletary SE, Kuerer HM, Buchholz T, Ames FC, et al. A prospective trial of preoperative chemotherapy in resectable breast cancer: predictors of breast-conservation therapy feasibility. Ann Surg Oncol. 2002; 9: 228–234. PMID: 11923128
8. Helvie MA, Joynt LK, Cody RL, Pierce LJ, Adler DD, Merajver SD. Locally advanced breast carcinoma: accuracy of mammography versus clinical examination in the prediction of residual disease after chemotherapy. Radiology. 1996; 198: 327–332. PMID: 8596826
9. Vinnicombe SJ, MacVicar AD, Guy RL, Sloane JP, Powles TJ, Knee G, et al. Primary breast cancer: mammographic changes after neoadjuvant chemotherapy, with pathologic correlation. Radiology. 1996; 198: 333–340. PMID: 8596827
10. Ross BD, Chenevert TL, Kim B, Ben-Yoseph O. Magnetic resonance imaging and spectroscopy: Application to experimental neuro-oncology. Quart Magn Res Biol Med. 1994; 1: 89–106.
11. Hajnal JV, Doran M, Hall AS, Collins AG, Oatridge A, Pennock JM, et al. MR imaging of anisotropically restricted diffusion of water in the nervous system: technical, anatomic, and pathologic considerations. J Comput Assist Tomogr. 1991; 15: 1–18. PMID: 1987175
12. Le Bihan D. Theoretical principles of perfusion imaging. Application to magnetic resonance imaging. Invest Radiol. 1992; 27 Suppl 2: S6–11. PMID: 1468877
13. Le Bihan D, Breton E, Lallemand D, Aubin ML, Vignaud J, Laval-Jeantet M. Separation of diffusion and perfusion in intravoxel incoherent motion MR imaging. Radiology. 1988; 168: 497–505. PMID: 3393671
14. Guo AC, Cummings TJ, Dash RC, Provenzale JM. Lymphomas and high-grade astrocytomas: comparison of water diffusibility and histologic characteristics. Radiology. 2002; 224: 177–183. PMID: 12091680
15. Lang P, Wendland MF, Saeed M, Gindele A, Rosenau W, Mathur A, et al. Osteogenic sarcoma: noninvasive in vivo assessment of tumor necrosis with diffusion-weighted MR imaging. Radiology. 1998; 206: 227–235. PMID: 9423677
16. Lyng H, Haraldseth O, Rofstad EK. Measurement of cell density and necrotic fraction in human melanoma xenografts by diffusion weighted magnetic resonance imaging. Magn Reson Med. 2000; 43: 828–836. PMID: 10861877
17. Sugahara T, Korogi Y, Kochi M, Ikushima I, Shigematu Y, Hirai T, et al. Usefulness of diffusion-weighted MRI with echo-planar technique in the evaluation of cellularity in gliomas. J Magn Reson Imaging. 1999; 9: 53–60. PMID: 10030650
18. Chenevert TL, McKeever PE, Ross BD. Monitoring early response of experimental brain tumors to therapy using diffusion magnetic resonance imaging. Clin Cancer Res. 1997; 3: 1457–1466. PMID: 9815831
19. Galons JP, Altbach MI, Paine-Murrieta GD, Taylor CW, Gillies RJ. Early increases in breast tumor xenograft water mobility in response to paclitaxel therapy detected by non-invasive diffusion magnetic resonance imaging. Neoplasia. 1999; 1: 113–117. PMID: 10933044
20. Poptani H, Puumalainen AM, Grohn OH, Loimas S, Kainulainen R, Yla-Herttuala S, et al. Monitoring thymidine kinase and ganciclovir-induced changes in rat malignant glioma in vivo by nuclear magnetic resonance imaging. Cancer Gene Ther. 1998; 5: 101–109. PMID: 9570301
21. Chenevert TL, Stegman LD, Taylor JM, Robertson PL, Greenberg HS, Rehemtulla A, et al. Diffusion magnetic resonance imaging: an early surrogate marker of therapeutic efficacy in brain tumors. J Natl Cancer Inst. 2000; 92: 2029–2036. PMID: 11121466
22. Chinnaiyan AM, Prasad U, Shankar S, Hamstra DA, Shanaiah M, Chenevert TL, et al. Combined effect of tumor necrosis factor-related apoptosis-inducing ligand and ionizing radiation in breast cancer therapy. Proc Natl Acad Sci U S A. 2000; 97: 1754–1759. PMID: 10677530
23. Hall DE, Moffat BA, Stojanovska J, Johnson TD, Li Z, Hamstra DA, et al. Therapeutic efficacy of DTI-015 using diffusion magnetic resonance imaging as an early surrogate marker. Clin Cancer Res. 2004; 10: 7852–7859. PMID: 15585617
24. Hamstra DA, Lee KC, Tychewicz JM, Schepkin VD, Moffat BA, Chen M, et al. The use of 19F spectroscopy and diffusion-weighted MRI to evaluate differences in gene-dependent enzyme prodrug therapies. Mol Ther. 2004; 10: 916–928. PMID: 15509509

25. Stegman LD, Rehemtulla A, Hamstra DA, Rice DJ, Jonas SJ, Stout KL, et al. Diffusion MRI detects early events in the response of a glioma model to the yeast cytosine deaminase gene therapy strategy. Gene Ther. 2000; 7: 1005–1010. PMID: 10871748

26. Lee KC, Moffat BA, Schott AF, Layman R, Ellingworth S, Juliar R, et al. Prospective early response imaging biomarker for neoadjuvant breast cancer chemotherapy. Clin Cancer Res. 2007; 13: 443–450. PMID: 17255264

27. Lee KC, Sud S, Meyer CR, Moffat BA, Chenevert TL, Rehemtulla A, et al. An imaging biomarker of early treatment response in prostate cancer that has metastasized to the bone. Cancer Res. 2007; 67: 3524–3528. PMID: 17440058

28. McConville P, Hambardzumyan D, Moody JB, Leopold WR, Kreger AR, Woolliscroft MJ, et al. Magnetic resonance imaging determination of tumor grade and early response to temozolomide in a genetically engineered mouse model of glioma. Clin Cancer Res. 2007; 13: 2897–2904. PMID: 17504989

29. Baba S, Isoda T, Maruoka Y, Kitamura Y, Sasaki M, Yoshida T, et al. Diagnostic and Prognostic Value of Pretreatment SUV in 18F-FDG/PET in Breast Cancer: Comparison with Apparent Diffusion Coefficient from Diffusion-Weighted MR Imaging. J Nucl Med. 2014.

30. Hahn SY, Ko EY, Han BK, Shin JH, Ko ES. Role of diffusion-weighted imaging as an adjunct to contrast-enhanced breast MRI in evaluating residual breast cancer following neoadjuvant chemotherapy. Eur J Radiol. 2014; 83: 283–288. doi: 10.1016/j.ejrad.2013.10.023 PMID: 24315957

31. Iwasa H, Kubota K, Hamada N, Nogami M, Nishioka A. Early prediction of response to neoadjuvant chemotherapy in patients with breast cancer using diffusion-weighted imaging and gray-scale ultrasonography. Oncol Rep. 2014; 31: 1555–1560. doi: 10.3892/or.2014.3025 PMID: 24535214

32. Jensen LR, Garzon B, Heldahl MG, Bathen TF, Lundgren S, Gribbestad IS. Diffusion-weighted and dynamic contrast-enhanced MRI in evaluation of early treatment effects during neoadjuvant chemotherapy in breast cancer patients. J Magn Reson Imaging. 2011; 34: 1099–1109. doi: 10.1002/jmri.22726 PMID: 22002757

33. Wu LM, Hu JN, Gu HY, Hua J, Chen J, Xu JR. Can diffusion-weighted MR imaging and contrast-enhanced MR imaging precisely evaluate and predict pathological response to neoadjuvant chemotherapy in patients with breast cancer? Breast Cancer Res Treat. 2012; 135: 17–28. doi: 10.1007/s10549-012-2033-5 PMID: 22476850

34. Atuegwu NC, Arlinghaus LR, Li X, Chakravarthy AB, Abramson VG, Sanders ME, et al. Parameterizing the Logistic Model of Tumor Growth by DW-MRI and DCE-MRI Data to Predict Treatment Response and Changes in Breast Cancer Cellularity during Neoadjuvant Chemotherapy. Transl Oncol. 2013; 6: 256–264. PMID: 23730404

35. Atuegwu NC, Arlinghaus LR, Li X, Welch EB, Chakravarthy BA, Gore JC, et al. Integration of diffusion-weighted MRI data and a simple mathematical model to predict breast tumor cellularity during neoadjuvant chemotherapy. Magn Reson Med. 2011; 66: 1689–1696. doi: 10.1002/mrm.23203 PMID: 21956404

36. Moffat BA, Chenevert TL, Meyer CR, McKeever PE, Hall DE, Hoff BA, et al. The functional diffusion map: an imaging biomarker for the early prediction of cancer treatment outcome. Neoplasia. 2006; 8: 259–267. PMID: 16756718

37. Hamstra DA, Chenevert TL, Moffat BA, Johnson TD, Meyer CR, Mukherji SK, et al. Evaluation of the functional diffusion map as an early biomarker of time-to-progression and overall survival in high-grade glioma. Proc Natl Acad Sci U S A. 2005; 102: 16759–16764. PMID: 16267128

38. Moffat BA, Chenevert TL, Lawrence TS, Meyer CR, Johnson TD, Dong Q, et al. Functional diffusion map: a noninvasive MRI biomarker for early stratification of clinical brain tumor response. Proc Natl Acad Sci U S A. 2005; 102: 5524–5529. PMID: 15805192

39. Meyer CR, Boes JL, Kim B, Bland PH, Zasadny KR, Kison PV, et al. Demonstration of accuracy and clinical versatility of mutual information for automatic multimodality image fusion using affine and thin-plate spline warped geometric deformations. Med Image Anal. 1997; 1: 195–206. PMID: 9873906

40. Galban CJ, Mukherji SK, Chenevert TL, Meyer CR, Hamstra DA, Bland PH, et al. A feasibility study of parametric response map analysis of diffusion-weighted magnetic resonance imaging scans of head and neck cancer patients for providing early detection of therapeutic efficacy. Transl Oncol. 2009; 2: 184–190. PMID: 19701503

41. Galban CJ, Han MK, Boes JL, Chughtai KA, Meyer CR, Johnson TD, et al. Computed tomography-based biomarker provides unique signature for diagnosis of COPD phenotypes and disease progression. Nat Med. 2012; 18: 1711–1715. doi: 10.1038/nm.2971 PMID: 23042237

42. Galban CJ, Chenevert TL, Meyer CR, Tsien C, Lawrence TS, Hamstra DA, et al. The parametric response map is an imaging biomarker for early cancer treatment outcome. Nat Med. 2009; 15: 572–576. doi: 10.1038/nm.1919 PMID: 19377487

43. Hamstra DA, Galban CJ, Meyer CR, Johnson TD, Sundgren PC, Tsien C, et al. Functional diffusion map as an early imaging biomarker for high-grade glioma: correlation with conventional radiologic response and overall survival. J Clin Oncol. 2008; 26: 3387–3394. doi: 10.1200/JCO.2007.15.2363 PMID: 18541899

44. Hamstra DA, Lee KC, Moffat BA, Chenevert TL, Rehemtulla A, Ross BD. Diffusion magnetic resonance imaging: an imaging treatment response biomarker to chemoradiotherapy in a mouse model of squamous cell cancer of the head and neck. Transl Oncol. 2008; 1: 187–194. PMID: 19043529

45. Malyarenko D, Galban CJ, Londy FJ, Meyer CR, Johnson TD, Rehemtulla A, et al. Multi-system repeatability and reproducibility of apparent diffusion coefficient measurement using an ice-water phantom. J Magn Reson Imaging. 2013; 37: 1238–1246. doi: 10.1002/jmri.23825 PMID: 23023785

46. Huang W, Li X, Chen Y, Li X, Chang MC, Oborski MJ, et al. Variations of dynamic contrast-enhanced magnetic resonance imaging in evaluation of breast cancer therapy response: a multicenter data analysis challenge. Transl Oncol. 2014; 7: 153–166. PMID: 24772219

47. Chenevert TL, Malyarenko DI, Newitt D, Li X, Jayatilake M, Tudorica A, et al. Errors in Quantitative Image Analysis due to Platform-Dependent Image Scaling. Transl Oncol. 2014; 7: 65–71. PMID: 24772209

48. Eisenhauer EA, Therasse P, Bogaerts J, Schwartz LH, Sargent D, Ford R, et al. New response evaluation criteria in solid tumours: revised RECIST guideline (version 1.1). Eur J Cancer. 2009; 45: 228–247. doi: 10.1016/j.ejca.2008.10.026 PMID: 19097774

49. Pickles MD, Gibbs JE, Lowry M, Turnbull LW. Diffusion changes precede size reduction in neoadjuvant treatment of breast cancer. Mag Res Imaging. 2006; 24: 843–847.

50. Chenevert TL, Galban CJ, Ivancevic MK, Rohrer SE, Londy FJ, Kwee TC, et al. Diffusion coefficient measurement using a temperature-controlled fluid for quality control in multicenter studies. J Magn Reson Imaging. 2011; 34: 983–987. doi: 10.1002/jmri.22363 PMID: 21928310

51. Bookstein FL. Principal Warps: Thin-plate splines and the decomposition of deformations. IEEE Transactions on Pattern Analysis and Machine Intelligence. 1989; 11: 567–585.

52. Boes JL, Hoff BA, Hylton N, Pickles MD, Turnbull LW, Schott AF, et al. Image registration for quantitative parametric response mapping of cancer treatment response. Transl Oncol. 2014; 7: 101–110. PMID: 24772213

53. Mills R. Self-diffusion in normal and heavy water in the range 1-45.deg. J Phys Chem. 1973; 77: 685–688.

54. Ellingson BM, Malkin MG, Rand SD, Connelly JM, Quinsey C, LaViolette PS, et al. Validation of functional diffusion maps (fDMs) as a biomarker for human glioma cellularity. J Magn Reson Imaging. 2010; 31: 538–548. doi: 10.1002/jmri.22068 PMID: 20187195

55. Lee KC, Bradley DA, Hussain M, Meyer CR, Chenevert TL, Jacobson JA, et al. A feasibility study evaluating the functional diffusion map as a predictive imaging biomarker for detection of treatment response in a patient with metastatic prostate cancer to the bone. Neoplasia. 2007; 9: 1003–1011. PMID: 18084607

56. Chenevert TL, Ross BD. Diffusion imaging for therapy response assessment of brain tumor. Neuroimaging Clin N Am. 2009; 19: 559–571. doi: 10.1016/j.nic.2009.08.009 PMID: 19959005

57. Padhani AR, Liu G, Koh DM, Chenevert TL, Thoeny HC, Takahara T, et al. Diffusion-weighted magnetic resonance imaging as a cancer biomarker: consensus and recommendations. Neoplasia. 2009; 11: 102–125. PMID: 19186405

58. Le Bihan D. Molecular diffusion nuclear magnetic resonance imaging. Magn Reson Q. 1991; 7: 1–30. PMID: 2043461

59. Le Bihan D. Diffusion MRI: what water tells us about the brain. EMBO Mol Med. 2014.

60. Weis JA, Miga MI, Arlinghaus LR, Li X, Chakravarthy AB, Abramson V, et al. A mechanically coupled reaction-diffusion model for predicting the response of breast tumors to neoadjuvant chemotherapy. Phys Med Biol. 2013; 58: 5851–5866. doi: 10.1088/0031-9155/58/17/5851 PMID: 23920113

61. Whisenant JG, Ayers GD, Loveless ME, Barnes SL, Colvin DC, Yankeelov TE. Assessing reproducibility of diffusion-weighted magnetic resonance imaging studies in a murine model of HER2+ breast cancer. Magn Reson Imaging. 2014; 32: 245–249. doi: 10.1016/j.mri.2013.10.013 PMID: 24433723

62. Ellingson BM, LaViolette PS, Rand SD, Malkin MG, Connelly JM, Mueller WM, et al. Spatially quantifying microscopic tumor invasion and proliferation using a voxel-wise solution to a glioma growth model and serial diffusion MRI. Magn Reson Med. 2011; 65: 1131–1143. doi: 10.1002/mrm.22688 PMID: 21413079

63. Hiramatsu R, Kawabata S, Furuse M, Miyatake S, Kuroiwa T. Identification of early and distinct glioblastoma response patterns treated by boron neutron capture therapy not predicted by standard

radiographic assessment using functional diffusion map. Radiat Oncol. 2013; 8: 192. doi: 10.1186/1748-717X-8-192 PMID: 23915330

64. Ma B, Meyer CR, Pickles MD, Chenevert TL, Bland PH, Galban CJ, et al. Voxel-by-voxel functional diffusion mapping for early evaluation of breast cancer treatment. Inf Process Med Imaging. 2009; 21: 276–287. PMID: 19694270

65. Li X, Kang H, Arlinghaus LR, Abramson RG, Chakravarthy AB, Abramson VG, et al. Analyzing Spatial Heterogeneity in DCE- and DW-MRI Parametric Maps to Optimize Prediction of Pathologic Response to Neoadjuvant Chemotherapy in Breast Cancer. Transl Oncol. 2014; 7: 14–22. PMID: 24772203